IJSGS

ISSN: 2488-9229
FEDERAL UNIVERSITY
GUSAU-NIGERIA

INTERNATIONAL JOURNAL OF SCIENCE FOR GLOBAL SUSTAINABILITY

Natural Convection Couette Flow in the Presence of Magnetic Field and Thermal Property

Omokhuale E. and Dange M. S.
Department of Mathematical Sciences, Federal University Gusau, P. M. B. 1001, Zamfara State, Nigeria.

Corresponding Author's Email: emmanuelomokhuale@yahoo.com

Received on: April, 2023 **Revised and Accepted on:** May, 2023 **Published on:** July, 2023

ABSTRACT

This article examines the natural convection Couette flow in a hydrodynamic viscous fluid that is electrically conductive due to the thermal radiation effect. The governing flow in this study is modelled in the form of partial differential equations (PDEs) in dimensional form with initial and boundary conditions and the Couette fluid model is also be used to characterize the fluid behavior. Then, using suitable non-dimensional quantities, the governing non-linear PDEs are transformed. Since the flow governing equations of the problem under study are extremely complex and complicated, techniques that complement experimental and theoretical fluid dynamics by providing alternative potentially cheaper means of testing fluid flow systems is employed. Therefore, the Finite Element Method (FEM) is used after discretization of the PDEs. With Graphs and tables, the effects of embedded thermo physical parameters of engineering interests associated with the flow quantities viz. velocity, temperature, concentration of the fluid were examined through series of numerical experiments and discussed. This research also analyzes and compares the results obtained by Omokhuale and Jabaka (2022b). It is interesting to report that an excellent agreement was established, thereby authenticating and validating the accuracy of FEM as a strong tool. According to the results of this study, the actions of thermal radiation on the thermal and momentum boundary layers for increasing values are significant, also, increasing the magnetic field parameter impedes the fluid movement due to the Lorentz force action.

Keywords: Natural convection; Magnetohydrodynamic (MHD); Thermal radiation; FEM; Couette flow.

1.0 INTRODUCTION

Convective flows have been thoroughly studied and have caused many different physical effects. The interest is due to the many functional applications modeled or approximated in porous media as transport phenomena. Such flows occur in a wide range of industrial applications, as well as in many natural circumstances such as geothermal mining, nuclear waste storage, groundwater flows, industrial and agricultural water distribution, oil recovery processes, thermal insulation engineering, pollutant dispersal in aquifers, electronic component cooling, packing reactors, food processing (Sharma and Gandhi, 2022). Many physical situations find the existence of convection flow such as in the study of environmental heat transfer processes and in the cooling of nuclear reactors etc. There are three (3) forms namely: free, mixed and forced. Natural convection is most significant owing to its usefulness in numerous engineering applications. For example, in an automatic control system that comprise of electrical and electronic components that is constantly subjected to periodic heating and cooled by natural convection process. Natural convection flow under the influence of gravitational force has been investigated most extensively because they occur frequently in nature as well as in science and engineering applications. When a heated surface is in contact with a fluid, the result of temperature difference causes buoyancy force, which induces the natural convection (Fagbade *et al.*, 2016). Magnetohydrodynamic (MHD) is the knowledge of motion of an electrically conducting fluid like molten iron, mercury, and plasma due to magnetic field. MHD flow has seen an extensive range of applications in the modern past and has gained significant interest owing to those in geophysical and cosmic fluid dynamics (Qiang, 2020).

The concept of the thermal radiation effect, which is the electromagnetic wave radiation that a surface generates because of its heat, is gaining growing attention, especially when a magnetic field is

applied, due to its relevance in constructing different advanced energy conversion systems capable of operating at high temperatures (Jamaludin *et al.* 2020). Some other practical applications include nuclear plants, solar technology, spacecraft aerodynamics, and so forth. To this end, several scholars have conducted research on the influence of thermal radiation in a variety of physical settings. Shah *et al.* (2023) elaborated on the influence of heat-dependent thermodynamic fluid properties in MHD Casson flow affected by the coexistence of thermal and chemical reactions. Ojemeri *et al*. (2023) proposed the hydro magnetic natural flow of an electrically conductive Casson fluid due to the thermal radiation impact in an upright porous channel. The functions of suction and injection on free convection across a constant-heat vertical porous channel in the coexistence of chemical processes and thermal radiation were analytically solved by Usman *et al.* (2022) using an implicit finite difference scheme. Omokhuale *et al.* (2019) reported unsteady heat and mass Magnetohydrodynamic (MHD) convective Couette flow with thermal radiation. They solved their problem numerically.

Couette flow in fluid dynamics refers to the laminar flow of a viscous fluid in the space between the two parallel plates, one of which moves relative to the other. This flow is driven by virtue of viscous drag force acting on fluid and the applied pressure gradient is parallel to the plate. Such flow was named after Maurice Marie Alfred Couette in the 19th Century. Couette motion is applied in Magnetohydrodynamics power generators and pumps, petroleum industry, polymer technology, purification or crude oil and fluid droplets sprays (Raju *et al.*, 2016). Kabir *et al.* (2023) examined the impact of suction/injection and permeability of porous materials on a steady natural convection Couette flow of a viscous incompressible fluid passing through a vertical porous plate.

FEM is a numerical technique used to obtain an approximate solution to boundary value problems as they consist of elliptic partial differential equations and the boundary conditions. It has been applied to many physical problems. Omokhuale and Jabaka (2022a) researched on the effect of heat source on unsteady hydromagnetic convective Couette flow of a viscous, electrically conducting and incompressible fluid is investigated. The effects of heat sink and radiation on unsteady hydromagnetic convective Couette flow of a viscous electrically conducting and incompressible fluid was studied by Omokhuale and Jabaka (2022b). The governing equations that describe the flow formation, heat and mass transfer are modeled as Partial Differential Equations (PDEs) and solved numerically using Finite FEM.

This research attempts to extend the work of Omokhuale and Jabaka (2022b) by incorporating the effects of thermal radiation, magnetic field and mass absorption parameters using FEM. With the help of line graphs, the deviations of different impacting parameters are thoroughly examined.

2.0 PROBLEM FORMULATION

We considered two-dimensional unsteady convective Couette flow of an electrically conducting fluid past a porous plate. The assumptions stated below were considered: (i) The x^*-axis and y^*- axis is taken along the plate in the vertical upward and normal direction to the plate respectively. (ii) The transverse magnetic field of uniform strength B_o is applied normal to the plate. (iii) The fluid has thermal property. The Boussinesq's approximation is taken for the flow. Premised on these assumptions, the unsteady flow is governed by the following partial differential equations.

Continuity equation:

$$\frac{\partial v^*}{\partial y^*} = 0 \tag{1}$$

Momentum equation:

$$\frac{\partial u^*}{\partial t^*} = v\frac{\partial^2 u^*}{\partial y^{*2}} + g\beta_1\left(T^* - T_b^*\right) + g\beta_2\left(C^* - C_b^*\right) - \frac{\sigma\mu_e^2 B_0^2}{\rho}\left(u^* - U_0 t^{*n}\right) \tag{2}$$

Heat equation:

$$\frac{\partial T^*}{\partial t^*}=\frac{k}{\rho Cp}\frac{\partial^2 T^*}{\partial y^{*2}}-\frac{1}{\rho Cp}\frac{\partial q_r}{\partial y^*}-\frac{Q_0}{\rho Cp}\left(T^*-T_b^*\right) \tag{3}$$

Mass equation:

$$\frac{\partial C^*}{\partial t^*}=D\frac{\partial^2 C^*}{\partial y^{*2}}-R_c^*\left(C^*-C_b^*\right)+Q_1\left(T^*-T_b^*\right) \tag{4}$$

The corresponding initial and boundary conditions are:

$$\left.\begin{aligned} &t^*\le 0: u^*=0, T^*=T_b^*, C^*=C_b^* \quad for \quad 0\le y^*\le b \\ &t^*>0: \begin{cases} u^*=U_0 t^{*n}, T^*=T_b^*, C^*=C_b^* & at\ y^*=0 \\ u^*=0, T^*=T_b^*, C^*=C_b^* & at\ \ y^*=b \end{cases} \end{aligned}\right\} \tag{5}$$

Applying the Rosseland approximation, the radiative heat flux q_r is defined as:

$$q_r=-\frac{4\sigma^*}{3k}\frac{\partial T^{*4}}{\partial y^*} \tag{6}$$

we assume that the difference in temperature within the flow are sufficiently small such that q_r may be presented as a linear function of T^*. Therefore, on expanding T^{*4} in Taylor series about T_b^* up to first order approximation will give

$$T^{*4}=T_b^*+4\left(T^*-T_b^*\right)T_b^{*3}=4T^*T_b^{*3}-3T_b^{*4} \tag{6}$$

Using Equations (5) and (6) in the last term of Equation (2), we got:

$$\frac{\partial q_r}{\partial y^*}=-\frac{16\sigma T_b^{*3}}{3k}\frac{\partial^2 T^*}{\partial y^{*2}} \tag{7}$$

Introducing Equation (7) into Equation (2), the heat equation becomes:

$$\frac{\partial T^*}{\partial t^*}=\frac{k}{\rho Cp}\frac{\partial^2 T^*}{\partial y^{*2}}+\frac{16\sigma T_b^{*3}}{3k^*\rho Cp}\frac{\partial^2 T^*}{\partial y^{*2}}-\frac{Q_0}{\rho Cp}\left(T^*-T_b^*\right) \tag{8}$$

We will Introducing the following dimensionless quantities in Equations (2), (3) and (4):

$$\left.\begin{aligned} u=\frac{u^*}{b}, y=\frac{y^*}{b}, t=\frac{t^*\nu}{b^2}, T=\frac{T^*-T_b^*}{T_w^*-T_b^*}, C=\frac{C^*-C_b^*}{C_w^*-C_b^*}, \end{aligned}\right\} \tag{9}$$

The dimensionless form of Equations (1), (3) and (8) when the dimensionless quantities in equation (9) is used are:

$$\frac{\partial^2 u}{\partial y^2}-\frac{\partial u}{\partial t}+GrT+GcC-M^2\left(u-Ft^n\right)=0 \tag{10}$$

$$\frac{1}{\Pr}\left(\frac{3R+4}{3R}\right)\frac{\partial^2 T}{\partial y^2}-\frac{\partial T}{\partial t}+ST=0 \tag{11}$$

$$\frac{1}{Sc}\frac{\partial^2 C}{\partial y^2}-\frac{\partial C}{\partial t}+R_mC-\gamma T=0 \tag{12}$$

initial and boundary conditions (4) in dimensionless forms are:

$$\left.\begin{aligned} &t \le 0 : u = 0, T = 0, C = 0 \quad for \quad 0 \le y \le b \\ &t > 0 : \begin{cases} u = Ft^n, T = 1, C = 1 \quad at\ y = 0 \\ u = 0, T = 0, C = 0 \quad at\ \ y = b \end{cases} \end{aligned}\right\} \tag{13}$$

Two cases are investigated, to obtain the solutions of Equations (10) to (12) subject to the initial and boundary conditions (13):

1. Impulsive movement of the plate at $y = 0$ (i.e., $n = 0$) and
2. Uniform accelerated movement of the plate at $y = 0$ (i.e., $n = 1$).

Case (I): Impulsive movement of the plate at $y = 0$:

Taking $n = 0$ in Equation (10), then the Equation (10) can be expressed as

$$\frac{\partial^2 u}{\partial y^2} - \frac{\partial u}{\partial t} + GrT + GcC - M^2\left(u - F\right) = 0 \tag{14}$$

and the corresponding boundary conditions (13) reduce to

$$\left.\begin{aligned} &t \le 0 : u = 0, T = 0, C = 0 \quad for \quad 0 \le y \le b \\ &t > 0 : \begin{cases} u = F, T = 1, C = 1 \quad at\ y = 0 \\ u = 0, T = 0, C = 0 \quad at\ \ y = b \end{cases} \end{aligned}\right\} \tag{15}$$

Case (II): Uniform accelerated movement of the plate at $y = 0$.

Taking $n = 1$ in Equation (10), then the Equation (10) can be written as

$$\frac{\partial^2 u}{\partial y^2} - \frac{\partial u}{\partial t} + GrT + GcC - M^2\left(u - Ft\right) = 0 \tag{16}$$

and the initial and boundary conditions (13) reduce to

$$\left.\begin{aligned} &t \le 0 : u = 0, T = 0, C = 0 \quad for \quad 0 \le y \le b \\ &t > 0 : \begin{cases} u = Ft, T = 1, C = 1 \quad at\ y = 0 \\ u = 0, T = 0, C = 0 \quad at\ \ y = b \end{cases} \end{aligned}\right\} \tag{17}$$

For practical engineering applications and the design of chemical engineering systems, quantities of interest viz. Skin-friction, Nusselt and Sherwood numbers which are necessary to compute. The skin-friction or the shear tress at the moving plate of the channel in dimensionless form is given by

$$\tau = -\left(\frac{\tau_w^*}{\rho u_0 \nu}\right)_{y^*=0} = -\left(\frac{\partial u}{\partial y}\right)_{y^*=0} \tag{18}$$

The rate of heat transfer at the moving hot plate of the channel in dimensionless form is illustrated by

$$Nu_0 = -x^* \frac{\left(\dfrac{\partial T^*}{\partial y^*}\right)_{y^*=0}}{T_w^* - T_b^*} \Rightarrow Nu_0\, \mathrm{Re}_x^{-1} = -\left(\frac{\partial T}{\partial y}\right)_{y=0} \tag{19}$$

Also, the rate of heat transfer on the stationary plate is given by

$$Nu_1 = -x^* \frac{\left(\dfrac{\partial T^*}{\partial y^*}\right)_{y^*=b}}{T_w^* - T_b^*} \Rightarrow Nu_1\, \mathrm{Re}_x^{-1} = -\left(\frac{\partial T}{\partial y}\right)_{y=1} \tag{20}$$

The Sherwood number at the moving plate of the channel in dimensionless form is given by

$$Sh = -x^* \frac{\left(\frac{\partial C^*}{\partial y^*}\right)_{y^*=0}}{C_w^* - C_b^*} \Rightarrow Sh\,\mathrm{Re}_x^{-1} = -\left(\frac{\partial C}{\partial y}\right)_{y=0} \tag{21}$$

where Re_x is the Reynold's number. The mathematical modeling of the problem is now done. So, equations (11), (12), (14) and (16) presents a coupled system of linear PDEs and these are to be solved with initial and boundary conditions (15) and (17). Therefore, finding the exact solutions are complicated, whenever it is possible. Thus, these equations are solved numerically by FEM.

3.0 NUMERICAL SOLUTIONS

The FEM is an efficient numerical and computational method to solving a variety of engineering and real-world problems. So many developers, researchers and users have recognized this method as one of the most powerful numerical analysis tools useful to analyze complex engineering problems. The simplicity, flexibility, computability and accuracy of the method make it significant in modeling and design process. This is because of the discretization of domain of the problem is done employing highly flexible elements or uniform or non-uniform patches that can be easily shown as complex shapes. The method vitally comprises the piecewise continuous functions in a systematic way that reduces the error in the solution.

The procedures involved in the finite element analysis as follows:
procedure 1: Discretization of the domain
procedure 2: Generation of the element equations
procedure 3: Assembling of the element equations
procedure 4: Imposition of the boundary conditions
procedure 5: Solution of assembled equations
Variational Formulation

The Variational formulation associated with Equations (10) to (12) over a typical two-noded linear element (y_e, y_{e+1}) is given by

$$\int_{y_e}^{y_{e+1}} z_1 \left[\left(\frac{\partial u}{\partial t}\right) - \left(\frac{\partial^2 u}{\partial y^2}\right) - Gr(T) - Gc(C) + M^2\left(u - Ft^n\right)\right] dy = 0 \tag{22}$$

$$\int_{y_e}^{y_{e+1}} z_2 \left[\left(\frac{\partial T}{\partial t}\right) - \frac{1}{\mathrm{Pr}}\left(\frac{3R+4}{3R}\right)\left(\frac{\partial^2 T}{\partial y^2}\right) - S(T)\right] dy = 0 \tag{23}$$

$$\int_{y_e}^{y_{e+1}} z_3 \left[\left(\frac{\partial C}{\partial t}\right) - \frac{1}{Sc}\left(\frac{\partial^2 C}{\partial y^2}\right) - R_m(C) + \gamma(T)\right] dy = 0 \tag{24}$$

where z_1, z_2 and z_3 are arbitrary test functions and may be seen as the variation in u, T and C respectively. When the order of integration was reduced, we got the following system of equation:

$$\int_{y_e}^{y_{e+1}} z_1 \left[z_1\left(\frac{\partial u}{\partial t}\right) + \left(\frac{\partial z_1}{\partial y^2}\right)\left(\frac{\partial u}{\partial y}\right) + \left(M^2\right)(z_1)u - (F)(z_1)t^n - (Gr)(z_1)T - (Gc)(z_1)C\right] dy$$
$$- \left[(z_1)\left(\frac{\partial u}{\partial y}\right)\right]_{y_e}^{y_{e+1}} = 0 \tag{25}$$

$$\int_{y_e}^{y_{e+1}} \left[(z_2)\left(\frac{\partial T}{\partial t}\right) - \frac{1}{\mathrm{Pr}}\left(\frac{3R+4}{3R}\right)\left(\frac{\partial z_2}{\partial y}\right)\left(\frac{\partial T}{\partial y}\right) - (S)(z_2)(T)\right] dy - \left[\left(\frac{z_2}{\mathrm{Pr}}\right)\left(\frac{\partial T}{\partial y}\right)\right]_{y_e}^{y_{e+1}} = 0 \tag{26}$$

$$\int_{y_e}^{y_{e+1}}\left[(z_3)\left(\frac{\partial C}{\partial t}\right)+\frac{1}{Sc}\left(\frac{\partial z_3}{\partial y}\right)\left(\frac{\partial C}{\partial y}\right)-(R_m)(z_3)(C)-\gamma(z_3)(T)\right]dy-\left[\left(\frac{z_3}{Sc}\right)\left(\frac{\partial C}{\partial y}\right)\right]_{y_e}^{y_{e+1}}=0 \qquad (27)$$

3.1 Finite Element Formulation:

The finite element model can be gotten from Equations (25) to (27) by substituting the finite element approximations of the form:

$$u=\sum_{k=1}^{2}u_k^e\xi_k^e, T=\sum_{k=1}^{2}T_k^e\xi_k^e \text{ and } \sum_{k=1}^{2}C_k^e\xi_k^e \qquad (28)$$

with $z_1=z_2=z_3=\xi_k^e\,(k=1,2)$, u_k^e, T_k^e and C_k^e are the velocity, temperature and concentration respectively at the k^{th} node of typical e^{th} element (y_e, y_{e+1}) and ξ_k^e are the shape functions for this element (Y_e, Y_{e+1}) and are taken as:

$$\xi_1^e=\frac{y_{e+1}-y}{y_{e+1}-y_e} \text{ and } \xi_2^e=\frac{y-y_e}{y_{e+1}-y_e},\ y_e\le y\le y_{e+1} \qquad (29)$$

This finite element model of the equations for

$$\begin{bmatrix}[P^{11}] & [P^{12}] & [P^{13}]\\ [P^{21}] & [P^{22}] & [P^{23}]\\ [P^{31}] & [P^{32}] & [P^{33}]\end{bmatrix}\begin{bmatrix}\{u^e\}\\ \{T^e\}\\ \{C^e\}\end{bmatrix}+\begin{bmatrix}[W^{11}] & [W^{12}] & [W^{13}]\\ [W^{21}] & [W^{22}] & [W^{23}]\\ [W^{31}] & [W^{32}] & [W^{33}]\end{bmatrix}\begin{bmatrix}\{u'^e\}\\ \{T'^e\}\\ \{C'^e\}\end{bmatrix}=\begin{bmatrix}\{a^{1e}\}\\ \{a^{2e}\}\\ \{a^{3e}\}\end{bmatrix} \qquad (30)$$

where $\{\{P^{mn}\},\{W^{mn}\}\}$ and $\{\{u^e\},\{T^e\},\{C^e\},\{u^e\},\{T^e\},\{C^e\},\{a^{me}\}\}\,(m=1,2,3)$ are the set of matrices of order 2×2 and 2×1 respectively and $'$ (dash) indicates $\frac{d}{dy}$.

These matrices are defined as follows:

$$P_{Ik}^{11}=\int_{y_e}^{y_{e+1}}\left[\left(\frac{\partial\xi_i^e}{\partial y}\right)\left(\frac{\partial\xi_k^e}{\partial y}\right)\right]dy+(M^2)\int_{y_e}^{ye+1}\left[(\xi_i^e)(\xi_k^e)\right]dy-Ft^n\int_{y_e}^{ye+1}(\xi_i^e)dy,$$

$$P_{ik}^{12}=-Gr\int_{y_e}^{ye+1}\left[(\xi_i^e)(\xi_k^e)\right]dy, P_{ik}^{13}=-Gc\int_{y_e}^{ye+1}\left[(\xi_i^e)(\xi_k^e)\right]dy, W_{ik}^{11}=\int_{y_e}^{ye+1}\left[(\xi_i^e)(\xi_k^e)\right]dy, W_{ik}^{12}=W_{ik}^{13}=0,$$

$$W_{ik}^{21}, W_{ik}^{23}=0, W_{ik}^{31}=W_{ik}^{32}=0, P_{ik}^{21}=0, P_{ik}^{31}=0, b_i^{1e}=\left[(\xi_i^e)\left(\frac{\partial u}{\partial y}\right)\right]_{y_e}^{y_{e+1}}$$

$$P_{ik}^{22}=\frac{1}{\Pr}\left(\frac{3R+4}{3R}\right)\int_{y_e}^{ye+1}\left[\left(\frac{\partial\xi_i^e}{\partial y}\right)\left(\frac{\partial\xi_k^e}{\partial y}\right)\right]dy, P_{ik}^{23}=-S\int_{y_e}^{ye+1}\left[(\xi_i^e)(\xi_k^e)\right]dy,$$

$$P_{ik}^{33} = \frac{1}{Sc}\int_{Y_e}^{Ye+1}\left[\left(\frac{\partial \xi_i^e}{\partial Y}\right)\left(\frac{\partial \xi_k^e}{\partial Y}\right)\right]dy,$$

$$W_{ik}^{22}\int_{y_e}^{ye+1}\left[\left(\xi_i^e\right)\left(\xi_k^e\right)\right]dy, P^{25} = R_m\int_{y_e}^{ye+1}\left[\left(\xi_i^e\right)\left(\xi_k^e\right)\right]dy, P^{26} = \gamma\int_{y_e}^{ye+1}\left[\left(\xi_i^e\right)\left(\xi_k^e\right)\right]dy$$

$$a_i^{2e} = \left[\left(\frac{\xi_i^e}{\Pr}\right)\left(\frac{3R+4}{3R}\right)\left(\frac{\partial T}{\partial Y}\right) - S\left(\xi_i^e\right)\right]_{y_e}^{y_{e+1}},\ a_i^{3e} = \left[\left(\frac{\xi_i^e}{Sc}\right)\left(\frac{\partial C}{\partial y}\right)\right]_{y_e}^{y_{e+1}} \text{ and } W_{ik}^{33} = \int_{y_e}^{ye+1}\left[\left(\xi_i^e\right)\left(\xi_k^e\right)\right]dy.$$

In one-dimensional space, linear element, quadratic element or element of higher order can be used. The entire flow domain is divided into 10,000 quadratic elements of equal size. Each element is three-noded, and as such the whole domain contains 20,001 nodes. At each node, three functions are to be evaluated: hence, after assembling of the element equations, we got a system of 80,004 equations which are linear. Thus, an iterative scheme must be employed in the solution. On imposing the boundary conditions, a system of equations was gotten which is solved by Gauss elimination method while maintaining an accuracy of 0.00001. A convergence criterion based on the relative difference between the current and previous iterations is used. After these differences satisfy the desired accuracy, the solution is assumed to have been converged and iterative process terminated. The Gaussian quadrature is implemented for solving the integrations. The code of the algorithm has been executed twice in MAPLE for cases 1 and 2. Excellent results was seen for all results.

3.2 Study of Grid Independence

In general, to study the grid independency/dependency, the mesh size is varied in order to check the solution at different mesh (grid) sizes and get a range at which there is no variation in the solutions.

4.0 DISCUSSION OF RESULTS

The implications of natural convection Couette flow in the presence of magnetic field and thermal property were studied. Furthermore, a Maple program is written to generate line graphs for the velocity, temperature and concentration profiles in other to provide a clear understanding of the problem at hand where the influence of diverse and major controlling factors such as: magnetic field effect M, thermal radiation parameter (R), thermal Grashof number (Gr), mass Grashof number (Gc), heat sink parameter (R), heat absorption parameter (γ), chemical reaction parameter (Rc), Prandit number ($\Pr$), Schmidt number (Sc). The default values selected for this present analysis are: $Pr = 0.71, Sc = 0.66, R = Rc = S = M = Gc = Gr = \gamma = 1$. The results obtained by Omokhuale and Jabaka (2022b) was compared with this current investigation. The comparison confirms an excellent agreement.

Figures 1 and 2 show the impacts of thermal and mass Grashof numbers on the velocity profiles. It is clear that, there is increase in the velocity because of the enhancement of thermal buoyancy force. Similarly, the peak value of the velocity increases rapidly near the porous plate and the decays smoothly for free steam velocity. It is further observed that the fluid velocity increases and the peak value is more distinctive due to increase in species buoyancy force. Thus, the velocity distribution attains a distinctive maximum value in the vicinity of the plate and then reduces properly to approach free stream value. The impact of magnetic field parameter on the velocity profiles is as shown in Figure 3. It is seen that, the velocity of the fluid falls with ascending magnetic field strength. This is due to the Lorentz force, which is present when a magnetic field is applied to an electrically conductive fluid and a resistance force is produced. This force causes the fluid flow to slow down as it approaches the plate. As a result, all other forces, including the Lorentz force, vanish when the fluid comes to rest. The impact of thermal radiation on the velocity of the fluid is plotted in Figure 4. It is evident from the plots that velocity rises as thermal radiation becomes significant. Figure 5 illustrates the impact of Prandtl number on the temperature profiles. From this Figure, it is depicted that the temperature becomes lower as

Prandtl number is increased. The impact of heat sink on the velocity profiles in the boundary layer is provided in Figure 6. It is viewed that, increase in the heat source parameter leads in fall of the momentum boundary layer of the fluid. Figure 7 shows the impact of thermal radiation on the temperature of the fluid. It is viewed that increasing values of thermal radiation parameter causes the fluid temperature to rise.

Figures 8 and 9 provide the concentration field because of variation in Schmidt number and chemical reaction parameter. It is understood that; the concentration of the fluid falls as the Schmidt number is increased and a similar trend is seen as chemical reaction rises. Physically, this occurs because increase in Sc means decrease of molecular diffusivity, which results in decrease of concentration boundary layer. Hence, the concentration of species is smaller for higher values of Sc. Figure 10 illustrates the impact of mass absorption on the concentration of the fluid. The concentration of the fluid increases for higher values of γ.

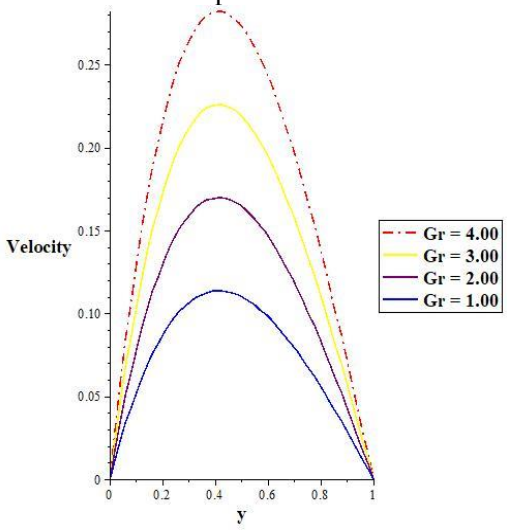

Figure 1: Impact of Gr on the velocity.

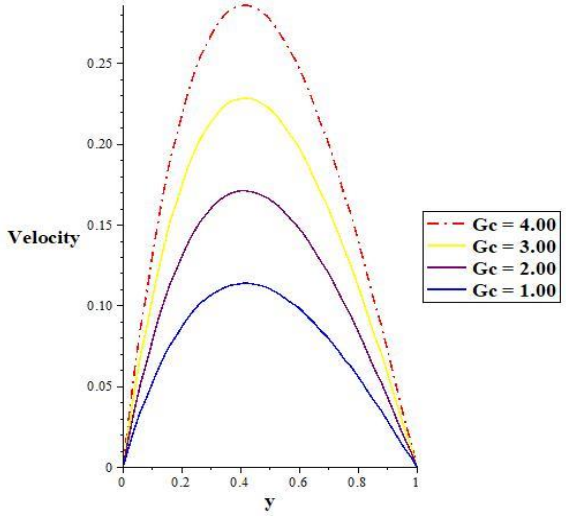

Figure 2: Impact of Gc on the velocity.

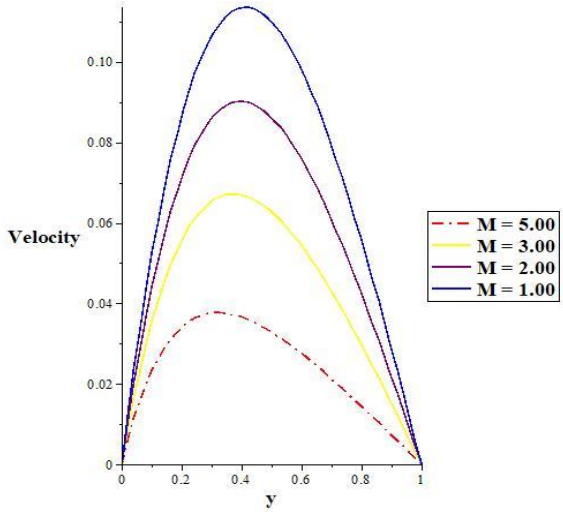

Figure 3: Impact of M on the velocity.

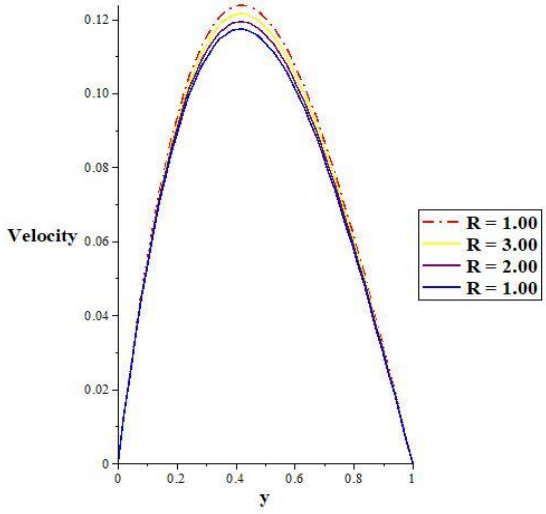

Figure 4: Impact of R on the velocity.

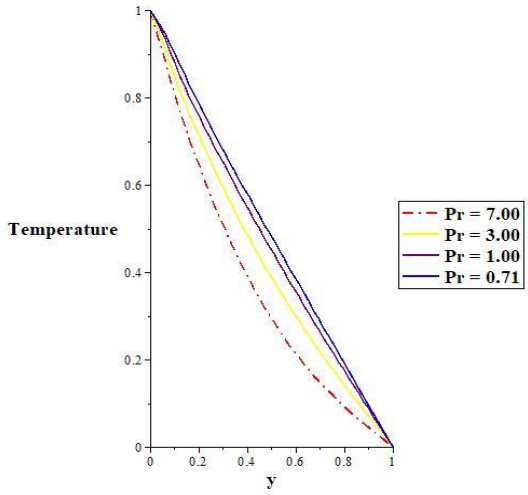

Figure 5: Impact of Pr on the temperature.

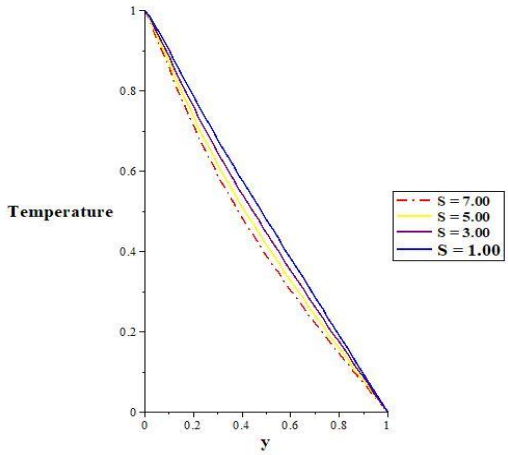

Figure 6: Impact of S on the temperature.

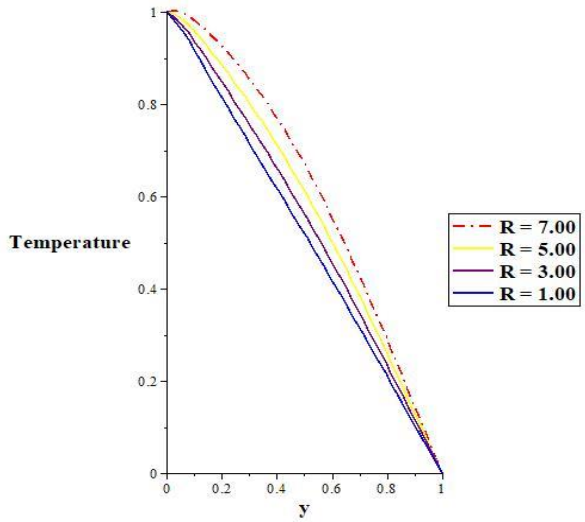

Figure 7: Impact of R on the temperature.

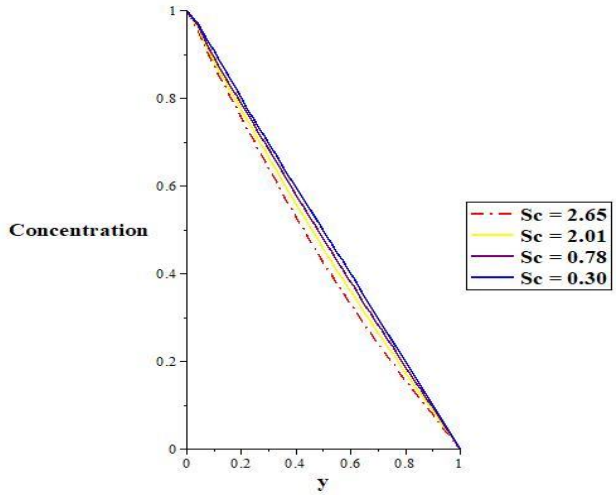

Figure 8: Impact of Sc on the concentration.

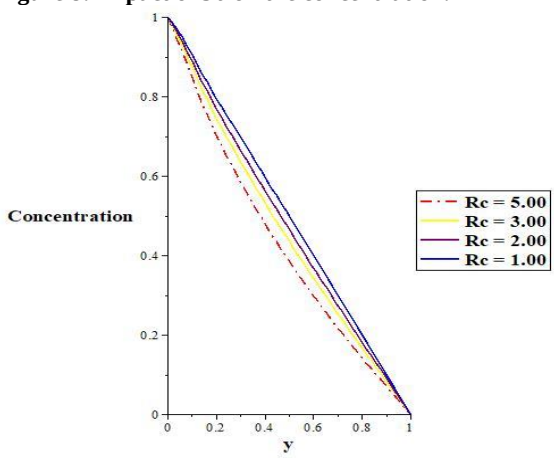

Figure 9: Impact of Rc on the concentration.

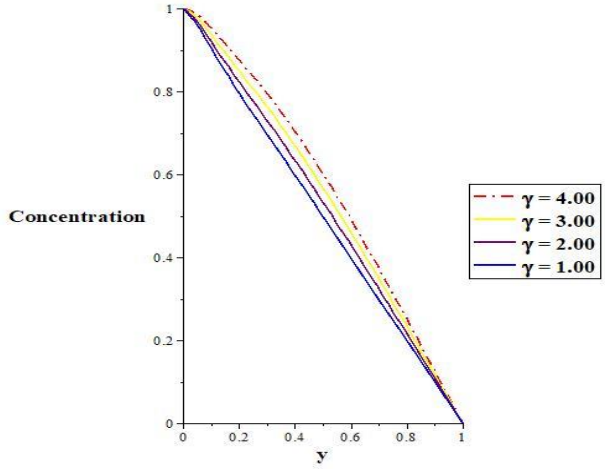

Figure 10: Impact of γ on the concentration.

5.0 CONCLUSION

The impacts thermal property and magnetic field on natural convection Couette flow has been investigated. One of the key achievements of this research is obtaining the same results as

Omokhuale and Jabaka (2022b). The major outcomes of this study are highlighted as follows:
i. The work of Omokhuale and Jabaka (2022b) was successfully recovered when the impact of mass absorption are neglected.
iii. The actions of thermal radiation on the thermal and momentum boundary layers for increasing values is significant.
iv. Increasing the magnetic number impedes the fluid movement due to the Lorentz force action.
v. Higher values of Prandit and Schmidt numbers lead to increase in the temperature and concentration of the fluid respectively.

6.0 ACKNOWLEDGEMENT

The authors are immensely grateful for the financial support received from the Tertiary Education Trust Fund (TETFund), Nigeria through Federal University Gusau, Nigeria Institutional Based Research (IBR) grant.

REFERENCES

Fagbade, A. I., Falodun, B. O., and Omowaye, A. J. (2018). MHD natural convection flow of viscoelastic fluid over an accelerating permeable surface with thermal radiation and heat source or sink: spectral homotopy analysis approach. *Ain Shams Engineering Journal*, *9*(4), 1029-1041.https://doi.org/10.1016/j.asej.2016.04.021.

Jamaludin A., Naganthran K., Nazar R., Pop I. (2020). Thermal radiation and MHD effect in the mixed convection flow of Fe3 O4 water Ferrofluid towards a nonlinear moving surface, Processes, 8, (95), https:doi.org.10.3390/pr8010095

Kabir, T. M., Umar, A. M. and Umar, L. (2023). Magnetohydrodynamics Free Convection Couette Flow and Heat Transfer Through a Vertical Porous Plate with Heat Generation and Absorption Effect. Dutse Journal of Pure and Applied Sciences (DUJOPAS), 9 (2a). 133 – 145. doi.org/10.4314/dujapas.v9i2a.13

Ojemeri G., Omokhuale E., Hamza M. M., Onwubuya I. O. and Shuaibu A. (2023). A Computational Analysis on Steady MHD Casson Fluid Flow Across a Vertical Porous Channel Affected by Thermal Radiation Effect. International Journal of Science for Global Sustainability, 9(1), https://doi.org/ 10.57233/ijsgs.v9i1.393

Omokhuale, E., Altine, M. M. and Yusuf, A. (2019). Unsteady heat and mass transfer Magnetohydrodynamic (MHD) convective Couette flow with thermal radiation using FEM. Caliphate Journal of Science and Technology, 1, 61 – 70.

Omokhuale, E. and Jabaka, M. L. (2022a). Unsteady convective Couette flow with heat source. International Journal of Science for Global Sustainability, 8(1), 25 – 37. https://doi.org/ 10.57233/ijsgs.v8i1.317

Omokhuale, E. and Jabaka, M. L. (2022b). Unsteady Convective Couette flow with heat sink and radiation effects. FUDMA Journal of Sciences, 6(1), 266 – 277. doi:10.33003/fjs-2022- 0601-873

Qiang, X., Siddique, I., Sadiq, K., and Shah, N. A. (2020). Double diffusive MHD convective flows of a viscous fluid under influence of the inclined magnetic field, source/sink and chemical reaction. Alexandria Engineering Journal, 59(6), 4171-4181. https://doi.org/10.1016/aej.2022.07.023.

Raju, R. S., Reddy, G. J., Rao, J. A. and Rashidi, M. M. (2016). Thermal diffusion and diffusion thermo effects on an unsteady heat and mass transfer Magnetohydrodynamic natural convection Couette flow using FEM. Journal of Computational Design and Engineering, 3, 349 – 362. https://doi.org/ 10.1016/j.jcde.2016.06.003

Shah S. A. G.A., Hassan A. Karamti H. (2023). Effect of thermal radiation on convective heat transfer in MHD boundary layer Carreau fluid with chemical reaction, Scientific Reports, 13, 4117, https:/doi.org/10.1038/s41598-023-31151-4

Sharma, B. K. and Gandhi, R. (2022). Combined effects of Joule heating and non-uniform heat source/sink on unsteady MHD mixed convective flow over a vertical stretching surface embedded in a Darcy-Forchheimer porous medium. Propulsion and Power Research, 11(2):276 – 292. https://doi.org/10.1016/j.jppr.2022.06.001.

Usman H., Tasi'u A. R. and Omokhuale E. (2022). Effects of suction/injection on free convective radiative flow in a vertical porous channel with

mass transfer and chemical reaction, International Journal for Science and Global Sustainability, 8(4), 28-37. https://doi.org/ 10.57233/ijsgs.v8i4.364x